

Universal characterization of epitope immunodominance from a multi-scale model of clonal competition in germinal centers

Federica Ferretti¹ and Mehran Kardar²

¹*Department of Chemical Engineering, Massachusetts Institute of Technology, Cambridge, Massachusetts 02139, USA*

²*Department of Physics, Massachusetts Institute of Technology, Cambridge, Massachusetts 02139, USA*

We introduce a multi-scale model for affinity maturation, which aims to capture the intra-clonal, inter-clonal and epitope-specific organization of the B cell population in a germinal center. We apply the Eigen’s model of quasispecies evolution in a random fitness landscape, where the desired multi-scale structure is reflected in the mutational connectivity of the B cell receptor (BCR) space, and on statistical characteristics of the fitness ensembles. Within this mathematical framework, we study the competition among classes of BCRs targeting different antigen epitopes, and construct an effective *immunogenic space* where epitope immunodominance relations can be universally characterized. We study how varying the composition of a mixture of antigens with variable and conserved domains allows for a parametric exploration of this space, and identify general principles for the rational design of two-antigen cocktails. We find that optimization of the cocktail composition must take into account possible statistical asymmetries between the two classes of BCRs targeting the two variants of the mutated epitope, as well as the evolutionary regime in which affinity maturation occurs.

I. INTRODUCTION

The molecular foundation of pathogen recognition and neutralization is the specific, high-affinity binding between antibodies and antigens [1, 2]. High affinity antibodies to any novel pathogen are generated via an accelerated evolutionary process called affinity maturation. Upon the encounter of foreign antigens, the immune system organizes a sophisticated learning machinery in the lymph nodes, where low-affinity naive B cells undergo iterated mutations and selections to acquire the desired specificity. When the B cells leave the germinal centers, they may become part of the memory repertoire or start secrete their receptors in the form of antibodies.

The fraction of an antigen protein recognized by an individual antibody or B cell receptor (BCR) —also known as epitope— is often considerably smaller than the overall size of natural antigens like viral structural proteins or other pathogen-derived molecules. As a result, from the perspective of B cell receptors, these antigens present a mosaic-like surface, where multiple, possibly overlapping, epitopes can be identified.

What antigenic drift —i.e. the immune evasion pattern of some pathogens— has revealed is that the primary antibody response is often focused towards a small subset of antigen sites, referred to as *immunodominant*, rather than being uniformly directed towards the entire set of recognition sites [3]. Consequently, these immunodominant epitopes are subject to heightened evolutionary pressure, since accumulating mutations on these sites increases the pathogen’s fitness and enables the mutants to escape the existing immune protection.

Universal vaccines for highly mutating pathogens aim at eliciting protection against many antigenically distant strains, by focusing the response towards unmutated, naturally immunorecessive epitopes. Various strategies have been explored so far in the pursuit of developing universal vaccines [4]: the underlying principle of these

approaches is to engineer vaccine formulations, immunogen design or protocols of administration to induce the production of broadly neutralizing antibodies, i.e. antibodies capable of neutralizing multiple variants of the pathogen by recognizing conserved regions in the antigen protein.

One of the most important aspects for the design of a universal vaccine is the choice of the immunogen cocktail. The rationale behind the use of antigen cocktails is that the simultaneous exposure to two or more antigen variants which share a set of conserved residues would help creating a competitive advantage for the broadly neutralizing antibodies. This idea has been employed in the SARS-CoV-2 bivalent booster, which incorporates antigens derived from the ancestral Wuhan strain and the omicron variant in equal parts [5, 6], as well as in the annual influenza vaccine, which contains a mixture of three influenza strains, one of which is periodically updated.

Clearly, understanding natural immunodominance hierarchies, how they change as the pathogen evolves, and how to manipulate them, is pivotal for vaccine development. In this paper we introduce a minimal model for affinity maturation which provides a novel universal framework to characterize epitope immunodominance, from which we can derive general guidelines on the rational design of antiviral cocktail vaccines. The key feature of the model, inspired by a long tradition of computational models of affinity maturation [7–12], is its multi-scale representation of clonal competition in a germinal center, which can occur at three different levels:

- (i) inter-class level: following the nomenclature used for SARS-CoV-2 antibodies, B cell receptors are categorized into *classes* based on the epitopes that they bind to [13].
- (ii) intra-class level: within each class, competition occurs among clonal lineages originating from different B cell ancestors (germlines);

- (iii) intra-clonal level: somatic hypermutations occurring during affinity maturation produce variability in the fitness of B cells within the same clonal family, enabling competition even at this level.

Within this framework, more immunodominant epitopes are associated with higher fixation probabilities of the corresponding BCR classes. We compute the fixation probability as an extreme value problem, and identify a restricted set of universal parameter combinations which modulate immunodominance in our model. In this setting, we also investigate how the epitope immunodominance relations can be manipulated by exposing the system to a cocktail of two antigens with varying relative concentrations. A more detailed mathematical description of the dynamical model is provided in Sec. II. Results for the construction of a universal immunodominance phase diagram and for the optimization problem for a bivalent antigen cocktail are presented in Sec. III; implications for future work are discussed in Sec. IV.

II. MODEL

1. A schematic description of affinity maturation

Affinity maturation is a key process in adaptive immunity, through which the B cell repertoire of an individual is expanded and refined in affinity upon the encounter of a foreign agent [14–16]. It encompasses an intricate series of reactions, involving various lymphocytes, cytokines and signaling pathways, which can be described, at a coarse-grained level, as an iterative two-step evolutionary process in which B cells undergo somatic hypermutation and competitive selection (see Fig. 1 for a schematic overview).

We adopt here a simplified model which describes the evolution process via parallel mutation, replication and death events. Let us assume that all the B cells compete for the same resources, i.e. interactions with follicular T cells and antigen capture. Competition can be then reintroduced by looking at the dynamics of the fraction of each BCR sequence in the germinal center, rather than their absolute number, as in Eigen’s well-known quasi-species model [17]. We consider each productive B cell receptor sequence as a distinct quasi-species, denoted by index $i = 1, \dots, N$. Replication, death and mutation events are described as simple first order reactions:

$$B_i \xrightarrow{\lambda_i} B_i + B_i, \quad B_i \xrightarrow{\delta} \emptyset, \quad B_i \xrightarrow{\mu_{ji}} B_j \quad (1)$$

where λ_i is a replication rate that depends on the affinity of the BCR to the presented antigen, δ is a constant death rate, and μ_{ji} is the effective mutation rate from sequence i to sequence j . For the sake of simplicity, we assume that mutations only occur at a constant rate μ between pairs of productive sequences that are at a Hamming distance of one [18].

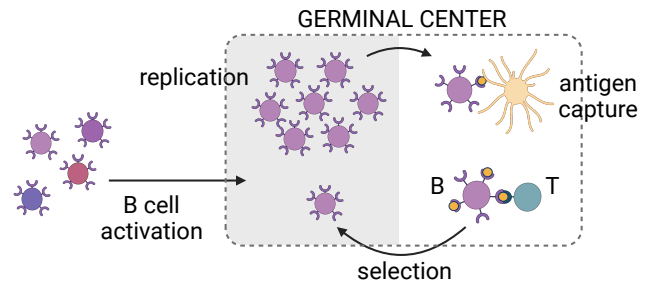


FIG. 1. Illustration of the main processes captured by our model. Affinity maturation starts with the activation of a pool of B cells, which are at least mildly reacting to the presented antigen. Activated B cells enter the germinal centers, where they undergo several iterations of a two-step process composed of replication with mutation (in the dark zone) and clonal selection (light zone). During selection, B cells compete with each other to capture antigen presented on the surface of follicular dendritic cells (yellow) and to interact with T helper cells. B-T signaling allows for the survival of the B cell, enabling migration to the dark zone, where it replicates and hypermutates again [7, 19]. We do not include in our model the process of differentiation of GC B cells into memory B cells and plasmablasts.

2. The B cell receptor space

Once the hopping rate is fixed, only the connectivity of the graph of allowed mutations needs to be specified. The number of somatic mutations that B cell receptors accumulate during affinity maturation is much smaller than the length of their sequence (typically of the order of 10 or less [20, 21]): let us encode in a binary string of length d the set of residues in the BCR sequence which can likely undergo such mutations. The resulting structure for the graph of accessible mutations from a starting reference sequence is then a d -dimensional hypercube, whose 2^d nodes of the hypercube represent all the potentially expressed BCRs within the same clonal lineage.

Since multiple germinal centers are recruited to initiate affinity maturation, the germinal center is described as a collection of disconnected hypercubes. The mutual distance between two distinct germinal centers is indeed typically larger than the mutational distance that can be covered by point-like somatic hypermutations during the process of affinity maturation.

3. Fitness landscape

Each hypercube in our model must be associated to a fitness landscape. Several theoretical models have been proposed over the decades to effectively model the topography of real fitness landscapes [22–26] and, since the advent of high-throughput sequencing techniques, an increasing number of them has been empirically reconstructed [27].

In the case of affinity maturation, the fitness landscape is shaped by the presented antigen. In order to achieve

reproducible affinity maturation, at least at the phenotypic level, the fitness of a BCR must be largely determined its binding affinity to the antigen. However, recent experimental results have demonstrated that other random effects can contribute to determining the effective fitness landscape we want to model, at our level of description where stochastic sub-processes—like antigen capture from follicular dendritic cells, antigen presentation on the B cell surface, and the encounter and interaction with T-helper cells—are not resolved [19].

Motivated by these findings, by the evidence of epistasis in the binding affinity of antibodies to antigens [28–31], and for the sake of tractability, we employ here a maximally epistatic model known as *House of Cards* or Random Energy Model (REM) [23, 24, 32, 33]. In the REM, the fitness values associated to each node in the graph are independent identically distributed (I.I.D.) random variables drawn from a given distribution $p(f)$. This probability distribution captures the immunogenic properties of the antigen from the point of view of the immune responders. However, different B cells can recognize different epitopes on the same antigen, with potentially different chemical and geometrical properties affecting the receptor binding affinities. We then group the clonal lineages into classes and associate a different fitness distribution to each class. The fitness landscapes imposed on hypercubes belonging to the same class are then independent quenched realizations of the same random energy model.

Figure 2 provides an illustrative representation of the structure of the GC space.

4. Evolution dynamics

Let n_i^α be the expected size of clone i belonging to lineage α ; from (1), we can derive a simple linear ODE for $\mathbf{n}(t) \in \mathbb{R}^{N \times M}$:

$$\partial_t n_i^\alpha = [f_i^\alpha \delta_{ij} + \mu \Lambda_{ij}] n_j^\alpha, \quad i = 1, \dots, N, \quad \alpha = 1, \dots, M, \quad (2)$$

where $N = 2^d$ is the number of nodes of each hypercube [34], and M is the number of clonal lineages in a single germinal center, typically of the order of $10 - 10^2$ [15]. The M clonal lineages are organized into a small number of classes, indexed by Γ , each of which contains m_Γ elements. The Λ_{ij} matrix indicates the Laplacian of the d -dimensional hypercube; the fitness is the net growth rate $f_i^\alpha = \lambda_i^\alpha - \delta^\alpha$. Initially the population is localized on the precursors' sequences: hence, without loss of generality, $n_i^\alpha(0) = \delta_{i,0} \forall \alpha$.

The model in Eq. (2) is known as parabolic Anderson model (PAM) [35]; analytical results for the PAM dynamics in the thermodynamic limit are known for several types of graphs, including hypercubes [36].

We are interested here in the evolution of B cell species

frequencies. This is a common way to introduce competition in evolutionary models with only first order reactions, which has been demonstrated to capture the behavior of classical fixed population models, such as the Wright-Fisher or Moran processes, in the limit of an infinite population [17]. Given the structure of the presented model, we can focus on competition at different levels:

(i) intra-clonal level:

$$\partial_t y_i^\alpha = [f_i^\alpha - \bar{f}^\alpha(t)] y_i^\alpha + \mu \sum_{j=1}^N \Lambda_{ij} y_j^\alpha, \quad (3)$$

where $y_i^\alpha(t) = n_i^\alpha(t) / \sum_{i=1}^N n_i^\alpha(t)$ is the fraction of identical clones i within the lineage, and $\bar{f}^\alpha(t) = \sum_{i=1}^N f_i^\alpha y_i^\alpha(t)$ is the average fitness of the clonal family;

(ii) intra-class level:

$$\partial_t X_\Gamma^\alpha = [\bar{f}^\alpha(t) - \Phi_\Gamma(t)] X_\Gamma^\alpha, \quad (4)$$

where $X_\Gamma^\alpha(t) = \sum_i n_i^\alpha(t) / \sum_{\alpha \in \Gamma} \sum_i n_i^\alpha(t)$ is the fraction of lineages in the class, and $\Phi_\Gamma(t) = \sum_{\alpha \in \Gamma} \bar{f}^\alpha(t) X_\Gamma^\alpha(t)$ is the population-averaged fitness of class Γ ;

(iii) inter-class level:

$$\partial_t z_\Gamma = [\Phi_\Gamma(t) - \bar{F}(t)] z_\Gamma, \quad (5)$$

where $z_\Gamma(t) = \sum_{\alpha \in \Gamma} \sum_i n_i^\alpha(t) / \sum_\alpha \sum_i n_i^\alpha(t)$ is the relative size of class Γ , and $\bar{F}(t) = \sum_\Gamma \Phi_\Gamma(t) z_\Gamma(t)$ is the total population-averaged fitness.

At the intra-clonal level, the system reaches at long times a state of mutation-selection balance, described by the ground state of the Anderson Hamiltonian. At the intra-class and inter-class level, due to the disconnected structure of the global graph, the stable fixed points of Eqs. (4)–(5) correspond to fixation of the asymptotically fittest quasi-species and extinction of the rest. The eventual dominance of a single clonal lineage in the germinal center (GC) population is consistent with experimental measurements, even though affinity maturation typically terminates before the germinal center becomes completely monoclonal [37, 38]. In this work, we will use the quenched average of $z_\Gamma(t)$ at long times to study epitope immunodominance from the GC response.

In the asymptotic-time limit, for any class Γ , z_Γ can only take values 0 or 1, depending on the realized collection of random fitness landscapes that describes the germinal center. The quenched average $\mathbb{E}[\lim_{t \rightarrow \infty} z_{\Gamma^*}(t)]$ is exactly equal to the fixation probability of class Γ^* , which can be computed as an extreme value problem:

Germinal Center:

$$\partial_t \mathbf{n}(t) = -\hat{H} \mathbf{n}(t)$$

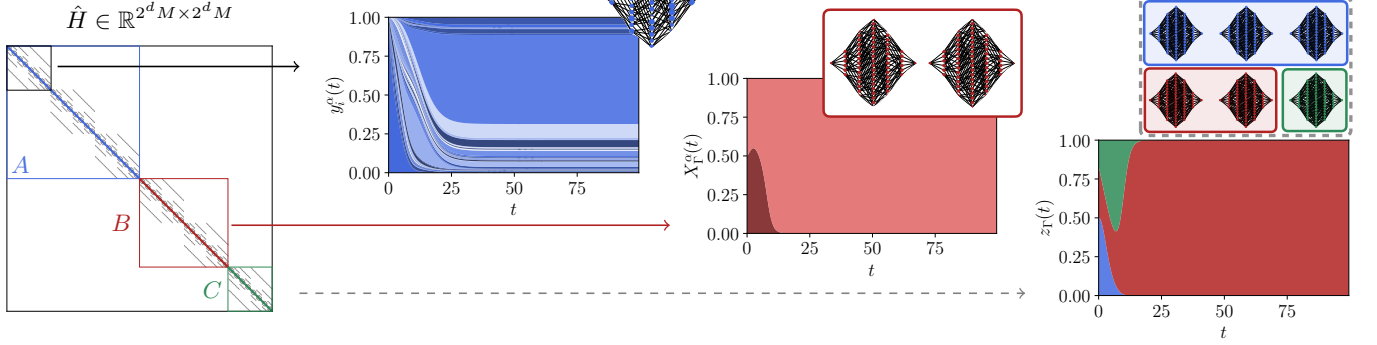


FIG. 2. Topography of the B cell receptor space. Clonal lineages are represented as hypercubes of effective dimension d , where mutations occur at a homogenous rate $1/d$. Each clonal lineage is uniquely associated to a class (here A , B or C), based on the targeted epitope. We impose on each epitope class a fitness landscape described by a random energy model on the hypercube with specific distributions. The germinal center dynamics is then described by a parabolic Anderson model (Eq. (2)), whose Anderson matrix has a block diagonal structure, with random diagonal entries drawn from the fitness distribution of the class corresponding to the block. Competition occurs at three different levels (cf. Eqs. (3)–(5)). Muller plots for the evolution of quasi-species at each level are shown for a quenched realization of a germinal center seeded by $M = 6$ germlines belonging to 3 distinct classes ($m_A = 3, m_B = 2, m_C = 1$).

$$\mathbb{E}[\lim_{t \rightarrow \infty} z_{\Gamma^*}(t)] = P_{fix, \Gamma^*} = m_{\Gamma^*} \int dx \rho_{\Gamma^*}(x) P_{\Gamma^*}(x)^{m_{\Gamma^*}-1} \prod_{\Gamma \neq \Gamma^*} P_{\Gamma}(x)^{m_{\Gamma}}, \quad (6)$$

where $\rho_{\Gamma}(x)$ is the probability density function (p.d.f.) of the asymptotic growth rate of the hypercube “mass,” and $P_{\Gamma}(x)$ is its cumulative density function (c.d.f.). The mass of hypercube α is defined as $N^{\alpha}(t) = \sum_i n_i^{\alpha}(t)$ and its asymptotic growth rate is

$$x^{\alpha} = \lim_{t \rightarrow \infty} \partial_t \log N^{\alpha}(t). \quad (7)$$

According to the linear nature of the PAM, the asymptotic growth rate of any hypercube mass is given by the ground state eigenvalue of the Anderson Hamiltonian, $H_{ij}^{\alpha} = -f_i^{\alpha} \delta_{ij} - \mu \Lambda_{ij}$. There is no general expression for the p.d.f. of this eigenvalue, but we can derive approximate expressions using first order perturbation theory in two limiting regimes.

Without loss of generality, let us fix the mutation rate to $\mu = 1/d$: all growth rates f_i^{α} are then measured in rescaled units, such that one mutation per unit time is expected. Let σ_{Γ} be the standard deviation of the fitness p.d.f. for any class Γ : the two limiting regimes are obtained when $d\sigma_{\Gamma} \ll 1$ (delocalized limit) or $d\sigma_{\Gamma} \gg 1$ (localized limit). The corresponding p.d.f.s for the ground state eigenvalues are (see App. A):

$$\rho_{\Gamma}^{del}(x) = \int d\mathbf{f} p_{\Gamma}(\mathbf{f}) \delta \left(x - \frac{1}{N} \sum_{i=1}^N f_i \right); \quad (8)$$

$$\rho_{\Gamma}^{loc}(x) = \int d\mathbf{f} p_{\Gamma}(\mathbf{f}) \delta \left(x - \max_{i=1 \dots N} \{f_i\} \right); \quad (9)$$

where $p_{\Gamma}(\mathbf{f}) = \prod_i p_{\Gamma}(f_i)$. When $d\sigma \ll 1$, the asymptotic growth rate can be identified with the average fitness on the hypercube, thanks to the delocalized nature of the ground state eigenvector. This regime corresponds to a scenario in which competition within the same lineage is not strong. By contrast, a strong selection-weak mutation regime corresponds to the localized limit, $d\sigma \gg 1$, where the asymptotic growth rate is identified with the extremum of the fitness values on the 2^d sites of the hypercube, where the ground state eigenvector is localized. We have confirmed numerically that this first order approximation works remarkably well for a wide range of working regimes, except in the strict vicinity of the localization transition, as demonstrated in App. A 2.

However, when the system is localized and d is very large, the dynamics is expected to be slow, with the system remaining stuck for long times in intermediate states. On an asymptotically large hypercube, the mass growth rate of the PAM eventually transitions from its initial value, corresponding to the fitness of the precursor, to its asymptotic value, corresponding to the extremum considered in Eq. (9), over a timescale that diverges as $d \rightarrow \infty$ [36]. Since affinity maturation has a finite duration, it may then be relevant to analyze a third regime, where the competition is determined by the initial mass growth rates. Here the p.d.f of the ground state eigen-

value in Eq. (6) is replaced by

$$\rho_{\Gamma}^{ini}(x) = p_{\Gamma}(x). \quad (10)$$

We remark that working in this regime corresponds to assuming that there exists a large separation of scales between the typical transition times for the mass growth rate of the hypercubes and intra-class fixation times — an assumption whose relevance needs to be justified by experimental evidence and a more exhaustive study of the full dynamics of the model.

Let us note that Eqs. (8)–(9) are valid for any fitness landscape, even in the presence of correlations. However, only when the fitness variables are independent and identically distributed, or weakly correlated with a finite correlation length $\xi \ll d$ [39, 40], ρ_{Γ}^{del} and ρ_{Γ}^{loc} are guaranteed to converge to universal laws as $N \rightarrow \infty$, for well-behaved $p_{\Gamma}(\mathbf{f})$. According to the generalized central limit theorem,

$$\rho_{\Gamma}^{del}(x) \approx h_{\alpha_{\Gamma}, \beta_{\Gamma}}\left(\frac{x - \mu_{\Gamma, N}}{\sigma_{\Gamma, N}}\right), \quad \text{for } N \gg 1, \quad (11)$$

where $h_{\alpha, \beta}(z)$ is a stable distribution whose canonical representation is given in terms of its characteristic function, for $0 < \alpha \leq 2$, $-1 \leq \beta \leq 1$ [41]. The parameters $\mu_{\Gamma, N}$ and $\sigma_{\Gamma, N}$ correspond respectively to the mean and standard deviation of the average of the N I.I.D. variables, when not undetermined. When the parent fitness variable has a finite σ_{Γ} , Eq. (11) reduces to the standard central limit theorem, where $\alpha = 2$ and β is irrelevant, and $h_{2, \beta}(z)$ corresponds to the Gaussian distribution.

Similarly, it is known from the theory of extreme value statistics that the c.d.f. of the maximum converges (for

most distributions) to one of three types of functions, rewritten in compact form as:

$$\int_{-\infty}^x du \rho_{\Gamma}^{loc}(u) \approx G_{\gamma_{\Gamma}}\left(\frac{x - b_{\Gamma, N}}{a_{\Gamma, N}}\right), \quad \text{for } N \gg 1, \quad (12)$$

where

$$G_{\gamma}(z) = \begin{cases} e^{-(1+\gamma z)^{-1/\gamma}} & \gamma \neq 0, 1 + \gamma z \geq 0 \\ e^{-e^{-z}} & \gamma = 0 \end{cases}, \quad (13)$$

and $b_{N, \Gamma}$ and $a_{N, \Gamma}$ are, respectively, average and standard deviation of $\max_{i=1 \dots N} \{f_i\}$ [42].

In summary, in both the localized and delocalized cases, the c.d.f. of the mass growth rate is of the form

$$P_{\Gamma}(x) \approx \Phi_{K_{\Gamma}}\left(\frac{x - \Delta_{\Gamma, N}}{\Sigma_{\Gamma, N}}\right), \quad (14)$$

where K_{Γ} is a set of parameters indicating the shape and skewness of the asymptotic growth rate distribution in the two considered regimes. Specifically, $K_{\Gamma} = (\alpha, \beta)$ in the delocalized limit, for the stable distribution $h_{\alpha, \beta}(x)$; $K_{\Gamma} = \gamma$ in the localized limit, for the extreme value distribution $G'_{\gamma}(x)$. The two sets of parameters $\Delta_{\Gamma, N}$ and $\Sigma_{\Gamma, N}$ represent respectively the shift and scale parameters of the variable of interest (average or maximum); they will depend on N and on the parameters of the parent fitness distribution.

Using the functional form (14) in Eq. (6), we obtain

$$P_{fix, \Gamma^*} \approx \int dx \frac{\partial}{\partial x} \left(\Phi_{K_{\Gamma^*}}\left(\frac{x - \Delta_{\Gamma^*, N}}{\Sigma_{\Gamma^*, N}}\right)^{m_{\Gamma^*}} \right) \prod_{\Gamma \neq \Gamma^*} \Phi_{K_{\Gamma}}\left(\frac{x - \Delta_{\Gamma, N}}{\Sigma_{\Gamma, N}}\right)^{m_{\Gamma}}, \quad N \gg 1. \quad (15)$$

Thanks to universality, the fixation probability of each class depends only on a handful of parameters which can in principle be derived from the fitness distributions $p_{\Gamma}(f)$, and on the germline abundance of the different BCR classes.

5. Antigen cocktails

To model affinity maturation in the context of an antigen cocktail, we must specify the fitness landscape imposed by individual antigens on any class of BCRs, as well as the rules by which these landscapes are combined.

Let us focus on a simplified scenario, where only two antigens are included in the vaccine, in relative proportions c and $1 - c$. We further assume that the antigens

are two variants of the same protein where we can distinguish, at a coarse-grained level, a mutated dominant epitope and a conserved subdominant epitope. The mutants are significantly distant in antigenic space, so that most of the antibodies generated after a primary immunization with one of the antigen may not neutralize the unseen antigen, as observed in the case of the SARS-CoV2 wild type strain and omicron variant [43, 44]. Hence, at a first approximation, cross-reactivity can only be achieved by targeting the conserved subdominant epitope.

In this framework, at least three classes of antibodies must be introduced: the classes targeting the mutant epitopes on antigen 1 and antigen 2, respectively named A and B , and the class targeting the shared epitope (C). Let $f^{\Gamma, a}$ indicate the fitness value of a BCR belonging to class $\Gamma \in \{A, B, C\}$ under exposure to antigen $a \in \{1, 2\}$. As an illustrative example, shown in Fig. 3, let us con-

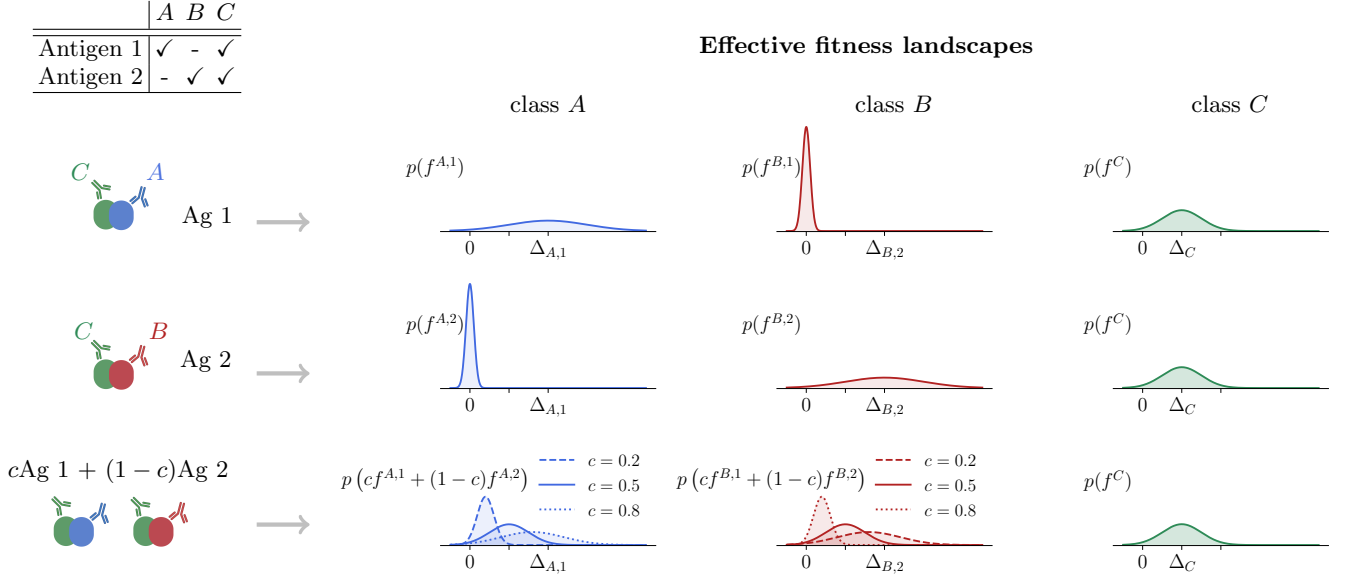


FIG. 3. The table summarizes the reactivity pattern of antigens and BCR classes. More precisely, reactivity is modeled by a Gaussian fitness distribution assigned to each antigen-BCR class pair. Non-reactive pairs have a narrow fitness distribution centered around zero, while reactive pairs have mostly positive fitness values. The effective “cocktail fitness landscape” is the weighted average of the fitness landscapes imposed by individual antigens, with weights equal to the relative antigen concentrations. The distribution of class C remains unaffected by c since the targeted epitope (in green) is the same on both antigens.

sider Gaussian distributions $\mathcal{N}(\mu_{\Gamma,a}, \sigma_{\Gamma,a})$. We can interpret $f_i^{\Gamma,a} dt$ as the probability to have a replication event for the BCR i in a time interval dt , conditioned to the encounter of antigen a . Then the marginal probability of a replication event per unit time, in the presence of multiple antigens, reads:

$$f_i^{\Gamma} = cf_i^{\Gamma,1} + (1-c)f_i^{\Gamma,2}. \quad (16)$$

This weighted average describes the effective fitness of the BCRs in the cocktail when all antigen types are presented homogeneously and abundantly on the follicular dendritic cells, so that each B cell, during its residency in the light zone, effectively samples their relative abundance. In the rest of this paper, we will adopt this assumption.

Similarly, the frequencies of activated precursors will be impacted by the composition of the cocktail. Let us assume that, for a fixed total amount of antigen, the expected number of precursors entering the GC is fixed to M , but the number of precursors of each class m_{Γ} depends on the original abundance ν_{Γ} of reactive B cells of class Γ in the repertoire and on the concentration of the targeted epitope. Imposing the condition $\sum_{\Gamma} m_{\Gamma} = M$,

we have:

$$\frac{m_A}{M} = \frac{c\nu_A}{c\nu_A + (1-c)\nu_B + \nu_C}; \quad (17)$$

$$\frac{m_B}{M} = \frac{(1-c)\nu_B}{c\nu_A + (1-c)\nu_B + \nu_C}; \quad (18)$$

$$\frac{m_C}{M} = \frac{\nu_C}{c\nu_A + (1-c)\nu_B + \nu_C}. \quad (19)$$

These combination rules for the fitness landscapes of the various BCR classes and for the frequencies of precursors entering the germinal center establish how varying the composition of an antigen cocktail translates into a parametric exploration of the effective parameter space which defines immunodominance.

For the sake of simplicity, let us assume that the fitness associated to each non-reactive antigen-BCR pair is exactly zero, while fitness values associated to reactive antigen-BCR pairs are mostly positive. In that case,

$$f_i^A = cf_i^{A,1}, \quad f_i^B = (1-c)f_i^{B,2}, \quad f_i^C = f_i^C, \quad (20)$$

and the same prescription also applies to the effective asymptotic growth rates of the hypercubes' mass. Therefore:

$$P_{fix,C}(c) \approx \int dx \frac{\partial}{\partial x} \left(\Phi_{K_C} \left(\frac{x - \Delta_{C,N}}{\Sigma_{C,N}} \right)^{m_C(c)} \right) \Phi_{K_A} \left(\frac{x - \Delta_{A,N}(c)}{\Sigma_{A,N}(c)} \right)^{m_A(c)} \Phi_{K_B} \left(\frac{x - \Delta_{B,N}(c)}{\Sigma_{B,N}(c)} \right)^{m_B(c)}, \quad (21)$$

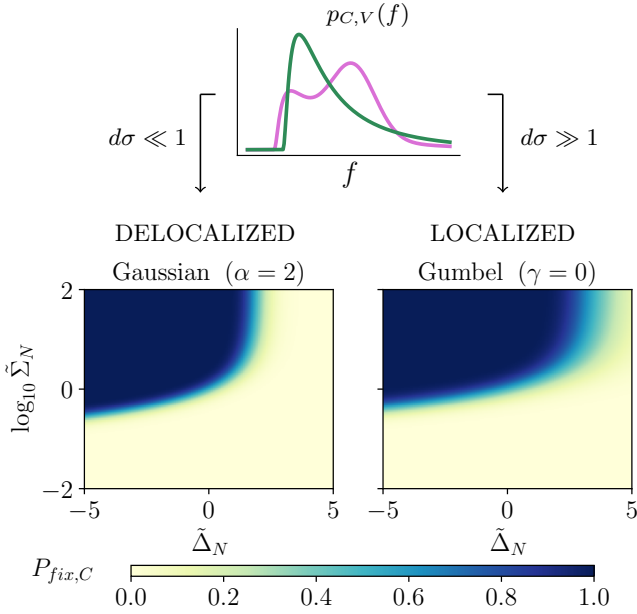


FIG. 4. Independently of the parent fitness distributions $p_{C,V}(f)$, in the two regimes $d\sigma \ll 1$ and $d\sigma \gg 1$ the c.d.f.s of the asymptotic mass growth rate $P_{C,V}(x)$ will take a universal form, for $N \gg 1$ (Eq. (14)). These c.d.f.s must be combined as in Eq. (15) to compute the fixation probability for the two-class problem. We show here plots of the fixation probability as a function of the dimensionless parameter combinations (24) in two example situations where the shape parameters of the two classes are equal. Specifically, we take Gaussian limit stable laws ($\alpha_C = \alpha_V = 2$) in the delocalized regime, and Gumbel extreme value distributions ($\gamma_C = \gamma_V = 2$) in the localized regime. In this plot, $m_V = m_C = 0.5M$, $M = 50$.

where, for any N ,

$$\Delta_{A,N}(c) = c\Delta_N^{A,1} : \Delta_{B,N}(c) = (1-c)\Delta_N^{B,2}; \quad (22)$$

$$\Sigma_{A,N}(c) = c\Sigma_N^{A,1}; \quad \Sigma_{B,N}(c) = (1-c)\Sigma_N^{B,2}. \quad (23)$$

The parameters of class C are independent of c because the epitope targeted by cross-reactive BCRs is unchanged on the two antigens.

III. RESULTS

1. The immunogenic space

The notion of immunogenicity indicates the general ability of an antigen to stimulate an immune response: as such, it depends on multiple factors, most of which contribute to activate components of the immune system exerting a non-epitope-specific auxiliary function. In our model, we only focus on *differences* in immunogenicity among epitopes presented during the same infection: these differences are encoded in the fitness distributions and in the relative abundance of germ lines of different classes which initiate the GC response. For any combination of these model parameters, we can compute the

fixation probability of any BCR class using Eq. (15) and identify the class with the highest fixation probability as the dominant one.

Let us first focus on the simplest (two-class) problem, where only two distinct epitopes are targeted by two distinct classes of BCRs, named V (variable) and C (conserved). We are interested in determining when each one of the epitopes is dominant or recessive. Plots of $P_{fix,C}$ for some example cases are shown in Fig. 4 as a function of the dimensionless combinations of parameters [45]

$$\tilde{\Delta}_N = \frac{\Delta_{V,N} - \Delta_{C,N}}{\Sigma_{C,N}} \quad \text{and} \quad \tilde{\Sigma}_N = \frac{\Sigma_{C,N}}{\Sigma_{V,N}}. \quad (24)$$

Assuming that the GC capacity M is constrained by the total antigen amount and resource availability, the variables of our problem are only $\tilde{\Delta}_N$, $\tilde{\Sigma}_N$, and m_C/M . These parameters represent the axes of a three-dimensional immunogenic space, where different *phases* can be identified, as the immunodominant epitope switches from C to V (cf. Fig. 4). This framework can be extended to multiple classes of BCRs targeting an increasing number of distinct epitopes.

The practical question is how to relate the parameters of the universal distributions, $\Delta_{\Gamma,N}$ and $\Sigma_{\Gamma,N}$, to the parameters of the parent fitness distributions? To answer this question, it is useful to resort to derivations of the stable limit laws and extreme value distributions based on the renormalization group (RG) method. This idea has been repeatedly explored in the literature [46–52] and used to derive finite-size corrections to the limit distributions, as well as the asymptotic scaling of the shift and scale parameters—corresponding to $\Delta_{\Gamma,N}$ and $\Sigma_{\Gamma,N}$ in our notation. We refer to Ref. [42] for a concise derivation of the flow equations in the space of probability density functions for the localized case. In the delocalized case, where deriving explicit flow equations for the rescaling parameters is more involved, we will focus only on the Gaussian case; other cases refer to parent fitness distributions with diverging second moments, which are not biologically relevant.

If μ_Γ and σ_Γ^2 are respectively the mean and variance of the original fitness variables of BCRs of class Γ in the delocalized regime, we know that, asymptotically, $\Delta_{\Gamma,N} = \mu_\Gamma$ and $\Sigma_{\Gamma,N} = \sigma_\Gamma/\sqrt{N}$. Identifying $\log N = s$, treated as a continuous variable for large N ,

$$\partial_s \Delta_\Gamma(s) \approx 0, \quad \partial_s \Sigma_\Gamma(s) \approx -\frac{1}{2} \Sigma_\Gamma(s). \quad (25)$$

Recalling the definition (24) for the two-class problem,

$$\partial_s \tilde{\Delta}(s) \approx \frac{1}{2} \tilde{\Delta}(s), \quad \partial_s \tilde{\Sigma}(s) \approx 0. \quad (26)$$

In the localized regime, $\Delta_{\Gamma,N}$ and $\Sigma_{\Gamma,N}$ can be computed if we know the cumulative density function

$$F_\Gamma(z) = \int_{-\infty}^z df p_\Gamma(f) \equiv e^{-e^{-\varphi_\Gamma(z)}}, \quad (27)$$

via the closed set of equations [42]

$$b_\Gamma(s) = \varphi_\Gamma^{-1}(s); \quad a_\Gamma(s) = b'_\Gamma(s); \quad (28)$$

$$\Delta_{\Gamma,N} = b_\Gamma(\log N); \quad \Sigma_{\Gamma,N} = a_\Gamma(\log N). \quad (29)$$

From Eqs. (28)–(29), the flow equations for $\tilde{\Delta}(s)$ and $\tilde{\Sigma}(s)$ read

$$\frac{\partial \tilde{\Delta}(s)}{\partial s} = \frac{1}{\tilde{\Sigma}(s)} - 1 - \gamma_C(s) \tilde{\Delta}(s), \quad (30)$$

$$\frac{\partial \tilde{\Sigma}(s)}{\partial s} = [\gamma_C(s) - \gamma_V(s)] \tilde{\Sigma}(s), \quad (31)$$

where $\gamma_\Gamma(s) = a'_\Gamma(s)/a_\Gamma(s) \rightarrow \gamma_\Gamma$ as $s \rightarrow \infty$. Asymptotically,

$$\tilde{\Sigma}_N \approx \tilde{\Sigma}_0 N^{\gamma_C - \gamma_V}, \quad (32)$$

$$\tilde{\Delta}_N \approx \tilde{\Delta}_0 N^{-\gamma_C} - \frac{1 - N^{-\gamma_C}}{\gamma_C} + \frac{N^{-\gamma_C}}{\gamma_V \tilde{\Sigma}_0} (N^{\gamma_V} - 1), \quad (33)$$

where the initial conditions $\tilde{\Sigma}_0 = a_C(0)/a_S(0)$ and $\tilde{\Delta}_0 = (b_S(0) - b_C(0))/a_C(0)$ are defined after the following relations [42]:

$$F_\Gamma(-a_\Gamma(0)/b_\Gamma(0)) = F'_\Gamma(-a_\Gamma(0)/b_\Gamma(0)) = e^{-1}. \quad (34)$$

The flow equations (26), (30) and (31) can be exploited to construct an immunodominance phase diagram in the space of ‘bare’ control parameters $\tilde{\Delta}_0, \tilde{\Sigma}_0$ —which can be directly reconstructed from the parent distribution $p_\Gamma(f)$ —rather than $\tilde{\Delta}_N, \tilde{\Sigma}_N$. The idea is to identify from these equations the stable fixed points and their basins of attraction, and to associate to each basin the asymptotic value of $P_{fix,C}$ computed at the corresponding fixed point.

Figure 5 depicts an illustration of the flow equations and of the resulting immunodominance phase diagrams in some special cases of interest. If we work in the delocalized regime and assume, as in Fig. 4, that the tails of the two parent fitness distributions are of the same type, so that the shape parameters associated to V and C converge to the same value at the same rate, then $\tilde{\Sigma}_\infty$ is a constant and $\tilde{\Delta}_\infty$ diverges, keeping the same sign as $\tilde{\Delta}_0$. Then we obtain only two asymptotic values for $P_{fix,C}$, respectively equal to 0 (for $\tilde{\Delta}_0 > 0$) or 1 (for $\tilde{\Delta}_0 < 0$). In the localized case, when $\gamma_V(s) = \gamma_C(s) \rightarrow \gamma$, $\tilde{\Sigma}$ is a constant and

$$\tilde{\Delta} = \frac{1}{\gamma} \left(1/\tilde{\Sigma} - 1 \right) \quad (35)$$

identifies a line of fixed points, for $\gamma \neq 0$, whose stability is determined by the sign of γ . When $\gamma < 0$ the points are unstable [53]: since $\lim_{\tilde{\Delta} \rightarrow \infty} P_{fix,C} = 0$ and $\lim_{\tilde{\Delta} \rightarrow -\infty} P_{fix,C} = 1$, the line of fixed points becomes a transition line between a phase where the C epitope is dominant and a phase where it is subdominant.

Let us finally note that in the $N \rightarrow \infty$ limit the parameter m_C/M , indicating the fraction of class C germlines in the GC, becomes irrelevant: the phase diagram is thus the same for all values of $m_C/M \in (0, 1)$, as long as $M \ll N$. Finite size corrections may however be important: it is known that the slow convergence to the asymptotic distribution in the size N of the data set is problematic for the quantitative application of extreme value theory to real situations [54]. In our problem, finite size effects may become especially non-negligible if the effective size of the uncorrelated sequence space explored by each clonal lineage is not too big, as it can happen in the case of short-lasting affinity maturation or if we allow for strongly correlated fitness landscapes.

2. Cocktail design

The immunogenic space construction introduced in Sec. III 1 can be used to investigate how and when antigen cocktails can be used to invert the natural immunodominance relations between conserved and highly mutable epitopes. We recall that, under the assumptions outlined in Sec. II 5, manipulating the relative antigen concentration c in a two-antigen cocktail describes a parametric exploration of the immunogenic space of the three-class problem, as described by Eq. (21). This space is higher-dimensional, but if we are only interested in the immunodominance of one epitope (e.g. the conserved epitope targeted by class C B cells), we can exploit a lower bound on $P_{fix,C}(c)$ that casts the parametric three-class problem into an effective 2-class problem:

$$P_{fix,C}^{3cl}(c) \geq P_{fix,C}^{2cl} \left(\tilde{\Delta}^{eff}(c), \tilde{\Sigma}^{eff}(c), m_C(c) \right) \quad (36)$$

Here $P_{fix,C}^{2cl}$ is the fixation probability of C against a single effective class V , representing the most successful of A and B , with effective parameters

$$\tilde{\Delta}^{eff}(c) = \frac{\max\{c\Delta_{A,1}, (1-c)\Delta_{B,2}\} - \Delta_C}{\Sigma_C}; \quad (37)$$

$$\tilde{\Sigma}^{eff}(c) = \frac{\Sigma_C}{\max\{c\Sigma_{A,1}, (1-c)\Sigma_{B,2}\}}. \quad (38)$$

Let us note that Eqs. (36)–(38) are valid for any N , even though the bound may not be equally tight. For the sake of simplicity, we work in the space of ‘bare’ parameters $(\tilde{\Delta}_0, \tilde{\Sigma}_0)$, where the immunodominance phase diagram exhibits a sharp transition.

From a comparison between the shape of the parametric curves described by Eqs. (37)–(38) and that of the transition line in the thermodynamic limit, we can gain insight on several questions of interest, i.e.: given a pair of antigens, what is the optimal cocktail formulation that maximizes the production of class C B cells? What is the tolerance to imperfect tuning of antigen concentration at the optimum? And what are the conditions under which the optimized cocktail can make an epitope which is naturally immunorecessive de facto immunodominant?

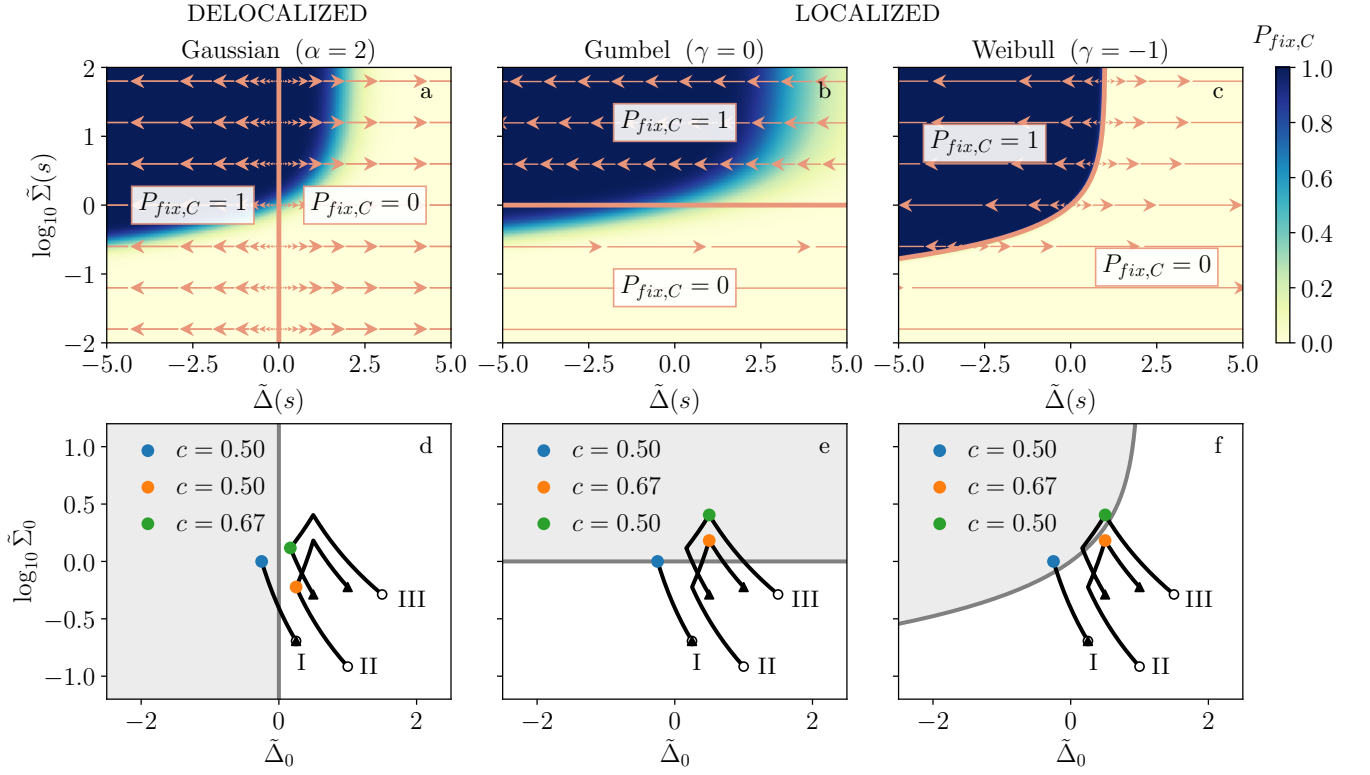


FIG. 5. **First row:** Identification of the basins of attraction of the RG flow equations. **a** - Delocalized Gaussian case, Eq. (26) **b-c** - Localized case, Eqs. (30)–(31), with $\gamma_C = \gamma_V = \gamma$. In the illustrated examples, there are no finite stable fixed points for $(\tilde{\Delta}(s), \tilde{\Sigma}(s))$. Hence the resulting immunodominance phase diagrams in the space of ‘measurable’ parameters $(\tilde{\Delta}_0, \tilde{\Sigma}_0)$ only exhibit two simple phases, corresponding to $P_{fix,C} = 0$ or $P_{fix,C} = 1$. **Second row:** Parametric exploration of the immunogenic space along the lower bound (36). The shaded region indicates the epitope immunodominant phase in the two-class setting. The black parametric curves are described by Eqs. (37)–(38), with parameters: (I) (symmetric case) $\Delta_{A,1} = \Delta_{B,2} = \Sigma_C$; $\Delta_C = 0.75\Sigma_C$; $\Sigma_{A,1} = \Sigma_{B,2} = 2\Sigma_C$; (II) (asymmetric Σ) $\Delta_{A,1} = \Delta_{B,2} = 1.5\Sigma_C$; $\Delta_C = \Sigma_{A,1} = 2.5\Sigma_C$; $\Sigma_{B,2} = 1.25\Sigma_C$; (III) (asymmetric Δ) $\Delta_{A,1} = \Sigma_C$; $\Delta_{B,2} = 2\Sigma_C$; $\Delta_C = 0.5\Sigma_C$; $\Sigma_{A,1} = \Sigma_{B,2} = 1.33\Sigma_C$. For each curve, the empty circle denotes the $c = 0$ point, the filled triangle the $c = 1$ point. **d** - Delocalized regime (Gaussian): here the transition line is vertical and the colored circles indicate the leftmost points along the parametric curves. These points correspond to $c = 1/2$ both in the symmetric case and when $\Sigma_{A,1} \neq \Sigma_{B,2}$. On the contrary, when $\Delta_{A,1} \neq \Delta_{B,2}$, the value of c at the leftmost point reflects the asymmetry in the parameters. **e** - Localized regime, $\gamma = 0$ (Gumbel): here the transition line is horizontal, and thus sensitive to imbalances of the kind $\Sigma_{A,1} \neq \Sigma_{B,2}$. **f** - Localized regime, $\gamma = -1/2$ (Weibull): colored points represent here the farthest points from the transition line, in the immunodominant phase of epitope C .

As regards the optimization of the cocktail composition, an obvious solution exists if the system is symmetric under exchange of c and $1 - c$, i.e. if $p_{A,1}(f) = p_{B,2}(f)$ and $\nu_A = \nu_B$. In that case, the optimum corresponds to a balanced mixture of antigens ($c^* = 1/2$) for any finite but large N , in both the considered evolutionary regimes (see Appendix B). When the symmetry is broken, the optimal composition will deviate from the even mixture, in order to balance the competition exerted by classes A and B on class C . The specific value of c^* is only implicitly determined for finite N in this asymmetric case, but a qualitative analysis can be extracted from the study of the immunodominance phase diagrams in the thermodynamic limit. When $\Delta_{A,1} \neq \Delta_{B,2}$ (curve III in Fig. 5 d–f), the asymmetry stretches the parametric lower bound curve in the horizontal direction: as a result, this asymmetry is best sensed in the delocalized case, where the transition line is perpendicular to that

direction. Similarly, the localized Gumbel case exhibits a transition line in the horizontal direction, making the system most sensitive to asymmetries in the Σ parameters of classes A and B , which stretch the parametric lower bound curve in the vertical direction (curve II in Fig. 5 d–f).

A sufficient condition for the inversion of the immunodominance hierarchy is that the parametric curve (37)–(38) crosses the manifold $P_{fix,C}^{2cl} = 1/2$ for some $c \in (0, 1)$. Clearly there is a restricted range of combinations of the original parameter values for the three BCR classes such that this crossing can be achieved. In the delocalized limit, the condition is restricted to the Δ_Γ parameters of the parent single-antigen fitness distributions, while in the localized limit, for $\gamma = 0$, it is restricted to the Σ_Γ parameters. For values of the shape parameter $\gamma < 0$, the conditions for inversion look generally more intricate, unless classes A and B have sym-

metric distributions for antigens 1 and 2.

This simple analysis also allows us to determine the tolerance to fluctuations in antigen concentrations. The exact amount of antigen of each type presented on the surface of follicular dendritic cells is indeed harder to control than the relative antigen concentration in the vaccine shot. This is especially true if the antigen cocktail is used as a boost after exposure to one of the antigens contained in the cocktail, because of the existence of strong feedback loops in the GC recall response [10, 55]. It is thus relevant to not only determine whether class C fixates for a given cocktail composition, but also the range of c values for which fixation still occurs with probability larger than a given threshold. If $N \gg 1$, the transition from fixation to extinction in the $(\tilde{\Delta}_0, \tilde{\Sigma}_0)$ plane is very sharp, both in the localized and delocalized regimes. Thus, the tolerance on the cocktail composition is roughly determined by how far the optimum is located from the transition line in any of the plots in Fig. 5.

The general properties discussed so far are robust to specific details of the problem, as they only arise from the identification of distinct well-known evolutionary regimes, which determine the relevant statistical properties of the problem. The bulk of the presented results is based on the assumption $N \gg 1$ and on long-time asymptotics, and we did not investigate in depth finite size or time corrections. In particular, finite time effects may well be important in the strongly localized limit where the effective size N of the explored sequence space is dramatically reduced (cf. Eq. (10)). In such case, since finite size corrections also extend to the third axis of the immunogenic space —i.e. germline abundance—, cocktail optimization becomes sensitive to possible imbalances in the relative germline abundances, with greater sensitivity exhibited for smaller N .

IV. CONCLUSION

Understanding the immunodominance relations among distinct epitopes is of paramount importance for developing universal vaccines against highly mutable pathogens and for studying pathogen coevolution in immunized hosts or populations. We proposed here a simple framework to characterize these immunodominance hierarchies, based on a coarse-grained statistical description of epitope-specific fitness landscapes for germinal-center B cells.

Epitope immunodominance arises from a combination of intrinsic characteristics of the epitopes themselves (such as chemical specificity, abundance on the antigen and their steric accessibility to immune cells) and statistical features of the B cell repertoire [56, 57]. Interestingly, epitope immunodominance seems to be a property of the pathogen, only slightly affected by individual or organismal particularities [58], suggesting that we can attempt to statistically describe immunodominance from the point of view of immune responders in a unique, non-

personalized way. In our model, the main factors affecting immunodominance are captured by associating distinct random fitness landscapes to distinct B cell classes (categorized by the epitope they bind to), and by introducing an explicit parameter that represents the typical precursor abundance for each epitope in the germinal center.

Our analysis reveals that, as the dimension of the genotypic space explored during affinity maturation increases, the details of the problem become less and less important and universality holds—at least in evolutionary regimes that are far from the localization transition. At long times, the impact of the precursor cell abundance vanishes (provided that the number of precursors per class remains sufficiently large for our deterministic approximation) and the average GC population becomes insensitive to the details of the fitness distributions of the various antibody classes. The fixation probability of any class, serving as a proxy for the immunogenic advantage of the targeted epitope, ultimately depends on a small, universally defined set of parameters. This set of parameters defines what we refer to as *immunogenic space*, where a phase transition occurs between immuno-dominant and immuno-recessive states for each considered epitope.

While comprehensive datasets enabling a systematic comparison of these parameters across various epitopes are currently lacking, recent advances in epitope mapping and deep mutational scanning techniques indicate the potential for their acquisition and analysis [28, 59, 60]. An ideal dataset for our framework would consist of high-throughput measurements of B cell receptor binding affinities to selected epitopes. Such a dataset would enable us to represent viral variants as points in this immunogenic space and offer valuable insights into viral evolution and the rational design of antigen cocktails. By assuming simple rules for combining single-antigen landscapes into a cocktail, our phase diagram representation highlights the conditions under which immunodominance relations can potentially be inverted. This insight might explain why cocktail-based vaccine formulations exhibit varying degrees of success in eliciting broadly neutralizing antibodies against different viruses, such as HIV or influenza [12, 61]. Furthermore, our representation can provide general guidelines for optimizing cocktail formulations based on the asymmetries in the effective immunogenicity parameters of non-conserved epitopes.

In conclusion, we believe that the framework we have proposed presents a promising avenue for a deeper understanding, prediction, and manipulation of immunodominance relations within the context of affinity maturation. To fully realize its potential, an invaluable input would be given by high-throughput experimental data that capture without bias the coarse-grained statistical properties of epitope binding affinities.

ACKNOWLEDGMENTS

We warmly thank Arup Chakraborty for suggesting the research problem and engaging in insightful discussions. MK acknowledges support from NSF grant DMR-2218849. Fig. 1 and Fig. 3 were created with BioRender.com

Appendix A: Ground state eigenvalue distribution for the Anderson model on the hypercube

1. First order perturbation theory

For each clonal lineage α , we have from (2)

$$H_{ij}^\alpha = -f_i^\alpha \delta_{ij} - \frac{1}{d} \Lambda_{ij}, \quad \Lambda_{ij} = -d\delta_{ij} + A_{ij}, \quad (\text{A1})$$

where A_{ij} is the adjacency matrix of the d -dimensional hypercube. Without loss of generality, let us take a zero-mean random diagonal and call σ the scale parameter of the I.I.D. variables, however defined (e.g. standard deviation, when not diverging). Let us define $\tilde{f}_i^\alpha = f_i^\alpha / \sigma$ a new random fitness variable with the same type of distribution but unit scale. The parameter that controls the Anderson localization transition is $d\sigma = \epsilon$, with $\epsilon_c \sim O(1)$. Two limiting regimes can be identified:

- $d\sigma = \epsilon \ll 1$ — delocalized regime. We can rewrite

$$H_{ij}^\alpha = \frac{1}{d} (\epsilon H_{ij}^1 + H_{ij}^0), \quad (\text{A2})$$

where $H_{ij}^0 = -\Lambda_{ij}$ and $H_{ij}^1 = -\tilde{f}_i^\alpha \delta_{ij}$. Spectrum and eigenvectors of the unperturbed Hamiltonian are exactly known for the d -dimensional hypercube. However, at first order in perturbation theory we are only exploiting the knowledge of the unperturbed ground state eigenvalue, $\lambda_0^0 = 0$, and the associated eigenvector, $\mathbf{v}_0^0 = \frac{1}{\sqrt{N}}(1, 1, \dots, 1)$, which are common to any graph Laplacian. Given the structure of \mathbf{v}_0^0 , the first order correction for the

asymptotic growth rate is,

$$x = -\lambda_0 \simeq -\frac{1}{d} (\lambda_0^0 + \epsilon \lambda_0^1) = \frac{1}{N} \sum_{i=1}^N f_i^\alpha, \quad (\text{A3})$$

from which we obtain the distribution $\rho^{del}(x)$ in Eq. (8).

- $d\sigma = \epsilon \gg 1$ — localized regime. Let us rewrite:

$$H_{ij}^\alpha = \sigma (H_{ij}^0 + \epsilon^{-1} H_{ij}^1) \quad (\text{A4})$$

where the unperturbed Hamiltonian $H_{ij}^0 = (-\tilde{f}_i^\alpha + \sigma^{-1}) \delta_{ij}$ is already diagonal, with ground state localized on the site with the maximum fitness. The perturbation is $H_{ij}^1 = -A_{ij}$. Since the adjacency matrix has null diagonal entries, at first order we have no correction to the ground state eigenvalue, leading to

$$x \simeq -\max\{f_i^\alpha, i = 1, \dots, N\}. \quad (\text{A5})$$

Both results hold true even when the random energy landscape is correlated; what changes, in such case, is only how the distributions of the empirical mean and of the maximum are computed.

2. Quality of perturbative approximations

We compare in Fig. 6 the estimate of the fixation probability obtained using the first order perturbative approximation of the mass growth rate p.d.f.s with numerical results for the example case of a Gaussian REM on the hypercube. The first order approximation, which does not take into account any detail of the geometry of the mutation graph, beyond symmetry and homogeneity of mutation rates, works remarkably well for a wide range of values, except in the vicinity of the localization transition.

Appendix B: Symmetric optimization

When $P_{fix,C}(c) = P_{fix,C}(1-c)$, the symmetry of the problem imposes that $c = 1/2$ be a stationary point. That this stationary point is also a maximum and no spontaneous symmetry breaking occurs must be proved by the concavity of this function.

Let us rewrite Eq. (6) for the symmetric case:

$$P_{fix,C}(c) = m_C M \int dx \rho_C(x) P_C(x)^{m_C M - 1} P_A(x; c)^{m_A(c)M} P_B(x; c)^{m_B(c)M}, \quad (\text{B1})$$

where m_C is independent of c , and $m_A = \nu m_C$, $m_B =$

$(1-c)\nu m_C$, with $\nu = \nu_A/\nu_C = \nu_B/\nu_C$. Because of the

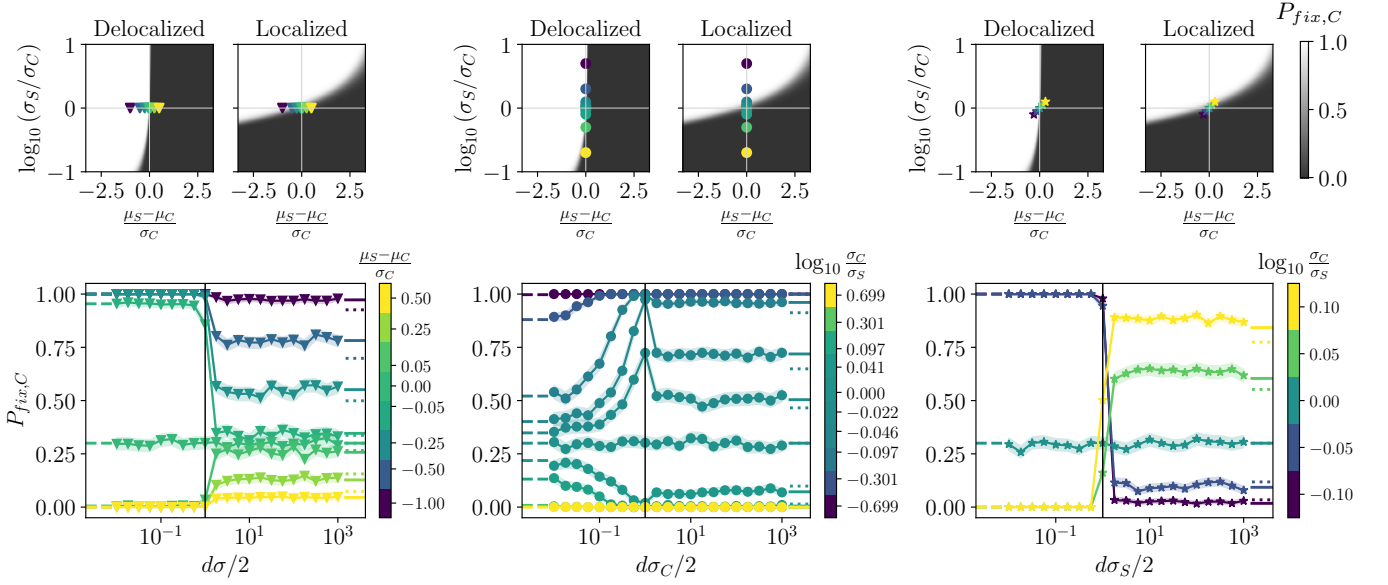


FIG. 6. **Top row:** Estimates of $P_{fix,C}$ from first order perturbation theory in the two-class setting. The fitness variables of the two classes, V and C , are distributed according to Gaussian p.d.f.s: $f_{\Gamma} \sim \mathcal{N}(\mu_{\Gamma}, \sigma_{\Gamma})$. **Bottom row:** Empirical fixation probability for the two-class problem, for varying disorder strength. As the disorder strength is varied, we interpolate between the delocalized and localized regimes on the first row. The empirical $P_{fix,C}$ is calculated as the fraction of times (over 1000 realizations) that the lowest ground state eigenvalue belongs to class C . On each realization, $M = 50$, $d = 10$, $N = 1024$, $m_C/M = 0.3$. The shaded areas correspond to 95% confidence interval for the inferred mean of a binomially distributed variable (with uniform prior). Dashed lines on the left of the plots correspond to the perturbative estimate in the delocalized approximation. Solid lines on the right correspond to the localized perturbative approximation using the exact p.d.f. for the maximum of $N = 1024$ Gaussian I.I.D. variables; dotted lines correspond to the same approximation using the Gumbel distribution (exact only for $N \rightarrow \infty$). The quality of the two approximations is very good for a large range of parameters. The vertical line $d\sigma = 2$ indicates the *bona fide* critical point, where the standard deviation of the fitness variables is equal to the spectral gap of the Laplacian. Interestingly, the interpolation between the two limiting values of $P_{fix,C}$ may be non-monotonic, for some points $((\mu_S - \mu_C)/\sigma_C, \sigma_C/\sigma_S)$, as shown in the center plot. This occurs because, if $\sigma_C/\sigma_S \neq 1$, it can happen that one of the two classes is localized and the other one is delocalized, favoring the fixation of the one with stronger disorder.

symmetry of the effective cocktail fitness distributions,

$$p_A(f; c) = p_B(f; 1 - c) \implies P_A(x; c) = P_B(x; 1 - c), \quad (\text{B2})$$

independently of the regime in which affinity maturation occurs. Working in the same setting as in the main text, where $f^A = cf^{A,1}$ and $f^B = (1 - c)f^{B,2}$, meaning that replication of a BCR is conditioned to the encounter of the reactive epitope, we can deduce that x^A/c and $x^B/(1 - c)$ are equal in probability. Here x^A and x^B represent the asymptotic mass growth rates of hypercubes in class A and B . For all the considered limiting regimes, the transformations that map f to x are indeed linear—extremum for localized regime at asymptotic times; identity for localized regime at early times; average for delocalized regime—, allowing us to rewrite the cumulative distribution of growth rates for classes A and B in terms of a reference distribution for the variable $\hat{x} = x^A/c$ or $\hat{x} = x^B/(1 - c)$, independent of c :

$$P_A(x; c) = \hat{P}\left(\frac{x}{c}\right); \quad P_B(x; c) = \hat{P}\left(\frac{x}{1 - c}\right). \quad (\text{B3})$$

We can now recognize that $\hat{P}(x)^{\nu m_C M} \equiv P(x)$ is the cumulative distribution of the maximum of a sequence of $\nu m_C M$ I.I.D. variables distributed as \hat{x} . Analogously, $m_C M \rho_C(x) P_C(x)^{m_C M - 1} \equiv \tilde{\rho}(x)$ is the p.d.f. of the maximum of $m_C M$ independent variables distributed as x^C . Therefore

$$P_{fix,C}(c) = \int dx \tilde{\rho}(x) P\left(\frac{x}{c}\right)^c P\left(\frac{x}{1 - c}\right)^{1 - c}. \quad (\text{B4})$$

It is not guaranteed, for any p.d.f. $\tilde{\rho}$ and any c.d.f. P , that (B4) is a concave function at $c^* = 1/2$. When the fixation probability is twice differentiable w.r.t. c , the general condition reads $\frac{\partial^2 P_{fix,C}}{\partial c^2} \Big|_{c^* = \frac{1}{2}} \leq 0$, with

$$\frac{\partial^2 P_{fix,C}}{\partial c^2} \Big|_{c^* = \frac{1}{2}} = \int dx \tilde{\rho}(x) 16x^2 P(2x) \frac{\partial^2 \log P(z)}{\partial z^2} \Big|_{z=2x}. \quad (\text{B5})$$

Nonetheless, if we identify $\hat{P}(a_N z + b_N)$ with $G_{\gamma}(z)$ in Eq. (13), the concavity condition can be easily proved. In any of the three cases, $\gamma = 0$, $\gamma < 0$ or $\gamma > 0$, the former identification implies that $P(a_N \nu m_C M z + b_N \nu m_C M)$ can also be identified with $G_{\gamma}(z)$. Hence we obtain, with a simple change of variables:

$$\left. \frac{\partial^2 P_{fix,C}}{\partial c^2} \right|_{c^*=\frac{1}{2}} = \int dx \tilde{\rho}_N(x) 16 \left(x + \frac{b_N}{2} \right)^2 \left(G_\gamma(z) \frac{\partial^2 \log G_\gamma(z)}{\partial z^2} \right) \Big|_{z=2x}, \quad \text{with} \quad \tilde{\rho}_N(x) = \int ds \tilde{\rho}(s) \delta \left(x - \frac{s - b_N}{a_N} \right). \quad (\text{B6})$$

We see from Eq. (13) that $G_\gamma(z)$ is not differentiable in \mathbb{R} when $\gamma \neq 0$; however we can rewrite in this case

$$G_\gamma(z) = \begin{cases} e^{-(1+\gamma z)^{-1/\gamma}} \Theta(1 + \gamma z), & \gamma > 0 \\ e^{-(1+\gamma z)^{-1/\gamma}} \Theta(1 + \gamma z) + \Theta(-1 - \gamma z), & \gamma < 0 \end{cases} \implies \log G_\gamma(z) = -(1 + \gamma z)^{-1/\gamma} \Theta(1 + \gamma z), \quad \text{for } \gamma \neq 0, \quad (\text{B7})$$

and approximate the Heaviside functions with smooth sigmoidal functions, e.g. $\Theta_l(s) = \frac{1}{\pi} \tan^{-1}(s/l) + 1/2$, such that $\Theta(s) = \lim_{l \rightarrow 0} \Theta_l(s)$. As a result,

$$\left. \frac{\partial^2 P_{fix,C}}{\partial c^2} \right|_{c^*=\frac{1}{2}} = \lim_{l \rightarrow 0} \begin{cases} - \int dx \tilde{\rho}_N(x) 16 \left(x + \frac{b_N}{2} \right)^2 e^{-2x - e^{-2x}}, & \gamma = 0; \\ - \int dx \tilde{\rho}_N(x) 16 \left(x + \frac{b_N}{2} \right)^2 G_\gamma(2x) (1 + 2\gamma x)^{-\frac{1}{\gamma}} \left[(1 + \gamma) (1 + 2\gamma x)^{-2} \Theta_l(1 + 2\gamma x) - \right. \\ \left. 2\gamma (1 + 2\gamma x)^{-1} \Theta'_l(1 + 2\gamma x) + \gamma^2 \Theta''_l(1 + 2\gamma x) \right], & \gamma \neq 0. \end{cases} \quad (\text{B8})$$

When $\gamma = 0$ $P_{fix,C}$ has a negative well-defined second derivative, which guarantees that $c^* = 1/2$ is a smooth maximum. On the contrary, when $\gamma \neq 0$, $P_{fix,C}(c)$ can have a kink at $c^* = 1/2$. By definition, $\lim_{l \rightarrow 0} \Theta_l(s) = \Theta(s)$, and $\lim_{l \rightarrow 0} \Theta'_l(s) = \delta(s)$. Hence the first term in the bracket has the sign of $1 + \gamma$. This term is finite when $\gamma > 0$, while it can diverge for $\gamma < 0$ —depending on whether and how fast $\tilde{\rho}_N(s)$ converges to 0 for $s \rightarrow -1/2\gamma$. The second term is null for any $\gamma > -1$. In the third term, Θ'_l formally converges to the derivative of a Dirac's delta function, which yields again a null integral for any $\gamma > -1$. In conclusion, $\left. \frac{\partial^2 P_{fix,C}}{\partial c^2} \right|_{c^*=\frac{1}{2}} \leq 0$ for any $\gamma > -1$, and it possibly diverges for $-1 < \gamma < 0$.

One can also make a hand-wavy argument for the concavity of $P_{fix,C}(c)$ in the delocalized regime: in the limit

$N \gg 1$, $\hat{P}(x)$ is a monotonically increasing function that varies very steeply between 0 and 1. Thus we can roughly approximate $\hat{P}(x) \simeq \theta(x - x^*)$: if $\nu m_C M \ll N$, this implies $P(x) \simeq \theta(x - x^*)$, at the same order of approximation. Therefore

$$P_{fix,C}(c) \simeq \int_{\max\{cx^*, (1-c)x^*\}} \tilde{\rho}(x), \quad (\text{B9})$$

implying $\arg \max_c P_{fix,C}(c) = \arg \min_c \max\{cx^*, (1-c)x^*\} = 1/2 \forall x^* \in \mathbb{R}_0$. The same line of reasoning can be applied to cases where we have more than two BCR classes competing with the cross-reactive one, which target equally immunogenic variants of the variable epitope. In this scenario, the optimum $\mathbf{c}^* = \arg \min_{\mathbf{c}: \sum_i c_i = 1} \max\{c_i x^*\}_{i=1, \dots, E}$ still corresponds to the balanced cocktail.

-
- [1] A. J. Charles, P. Travers, M. Walport, and M. J. Shlomchik, *Immunobiology: The Immune System in Health and Disease. 5th edition* (Garland Science, New York, 2001).
 - [2] G. Altan-Bonnet, T. Mora, and A. M. Walczak, Quantitative immunology for physicists, *Physics Reports* **849**, 1 (2020), quantitative immunology for physicists.
 - [3] M. O. Altman, D. Angeletti, and J. W. Yewdell, Antibody immunodominance: The key to understanding influenza virus antigenic drift., *Viral immunology* **31**, 10.1089/vim.2017.0129 (2018).
 - [4] C. W. Tan, S. A. Valkenburg, L. L. Poon, and L.-F. Wang, Broad-spectrum pan-genus and pan-family virus vaccines, *Cell Host and Microbe* **31**, 902 (2023).
 - [5] S. Chalkias, C. Harper, K. Vrbicky, S. R. Walsh, B. Es-sink, A. Brosz, N. McGhee, J. E. Tomassini, X. Chen, Y. Chang, A. Sutherland, D. C. Montefiori, B. Girard, D. K. Edwards, J. Feng, H. Zhou, L. R. Baden, J. M. Miller, and R. Das, A bivalent omicron-containing booster vaccine against covid-19, *New England Journal of Medicine* **387**, 1279 (2022).
 - [6] S. M. Scheaffer, D. Lee, B. Whitener, B. Ying, K. Wu, C.-Y. Liang, H. Jani, P. Martin, N. J. Amato, L. E. Avena, D. M. Berrueta, S. D. Schmidt, S. O'Dell, A. Nasir, G.-Y. Chuang, G. Stewart-Jones, R. A. Koup, N. A. Doria-Rose, A. Carfi, S. M. Elbashir, L. B. Thackray, D. K. Edwards, and M. S. Diamond, Bivalent sars-cov-2 mrna vaccines increase breadth of neutralization and protect against the ba.5 omicron variant in mice, *Nature Medicine* **29**, 247 (2023).
 - [7] M. Oprea and A. S. Perelson, Somatic mutation leads to efficient affinity maturation when centrocytes recycle back to centroblasts., *Journal of immunology* **158** **11**, 5155 (1997).
 - [8] S. Wang, J. Mata-Fink, B. Kriegsmann, M. Hanson, D. J. Irvine, H. N. Eisen, D. R. Burton, K. D. Wittrup, M. Kardar, and A. K. Chakraborty, Manipu-

- lating the selection forces during affinity maturation to generate cross-reactive hiv antibodies, *Cell* **160**, 10.1016/j.cell.2015.01.027 (2015).
- [9] M. Molari, K. Eyer, J. Baudry, S. Cocco, and R. Monasson, Quantitative modeling of the effect of antigen dosage on b-cell affinity distributions in maturing germinal centers, *eLife* **9**, e55678 (2020).
- [10] L. Yang, M. Van Beek, Z. Wang, F. Muecksch, M. Canis, T. Hatzioannou, P. D. Bieniasz, M. C. Nussenzweig, and A. K. Chakraborty, Antigen presentation dynamics shape the antibody response to variants like sars-cov-2 omicron after multiple vaccinations with the original strain, *Cell Reports* **42**, 10.1016/j.celrep.2023.112256 (2023).
- [11] K. G. Sprenger, J. E. Louveau, P. M. Murugan, and A. K. Chakraborty, Optimizing immunization protocols to elicit broadly neutralizing antibodies, *Proceedings of the National Academy of Sciences* **117**, 20077 (2020), <https://www.pnas.org/doi/pdf/10.1073/pnas.1919329117>.
- [12] L. Yang, T. M. Caradonna, A. G. Schmidt, and A. K. Chakraborty, Mechanisms that promote the evolution of cross-reactive antibodies upon vaccination with designed influenza immunogens, *Cell Reports* **42**, 10.1016/j.celrep.2023.112160 (2023).
- [13] C. O. Barnes, C. A. Jette, M. E. Abernathy, K.-M. A. Dam, S. R. Esswein, H. B. Gristick, A. G. Malyutin, N. G. Sharaf, K. E. Huey-Tubman, Y. E. Lee, D. F. Robbiani, M. C. Nussenzweig, A. P. West, and P. J. Bjorkman, Sars-cov-2 neutralizing antibody structures inform therapeutic strategies, *Nature* **588**, 682 (2020).
- [14] G. D. Victora and M. C. Nussenzweig, Germinal centers, *Annual Review of Immunology* **30**, 429 (2012), pMID: 22224772.
- [15] G. D. Victora and M. C. Nussenzweig, Germinal centers, *Annual Review of Immunology* **40**, 413 (2022), pMID: 35113731.
- [16] L. Mesin, J. Ersching, and G. D. Victora, Germinal center b cell dynamics, *Immunity* **45**, 471 (2016).
- [17] R. Cerf and J. Dalmau, *The Quasispecies Equation and Classical Population Models*, Probability Theory and Stochastic Modelling (Springer Cham, 2022).
- [18] This simplifying assumption overlooks the current understanding of the statistics of hypermutations, which have been observed to be far from uniform and to result into enrichment of specific nucleotide motifs [2, 62–64]. Nonetheless, we believe that a more realistic depiction of the mutational network will not significantly change our qualitative results and is not considered in this work.
- [19] G. D. Victora, T. A. Schwickert, D. R. Fooksman, A. O. Kamphorst, M. Meyer-Hermann, M. L. Dustin, and M. C. Nussenzweig, Germinal center dynamics revealed by multiphoton microscopy with a photoactivatable fluorescent reporter, *Cell* **143**, 10.1016/j.cell.2010.10.032 (2010/11/12).
- [20] K. G. C. Smith, A. Light, G. J. V. Nossal, and D. M. Tarlinton, The extent of affinity maturation differs between the memory and antibody-forming cell compartments in the primary immune response, *The EMBO Journal* **16**, 2996 (1997), <https://www.embopress.org/doi/pdf/10.1093/emboj/16.11.2996>.
- [21] W. Dejnirattisai, D. Zhou, H. M. Ginn, H. M. Duyvesteyn, P. Supasa, J. B. Case, Y. Zhao, T. S. Walter, A. J. Mentzer, C. Liu, B. Wang, G. C. Paesen, J. Slon-Campos, C. López-Camacho, N. M. Kafai, A. L. Bailey, R. E. Chen, B. Ying, C. Thompson, J. Bolton, A. Fyfe, S. Gupta, T. K. Tan, J. Gilbert-Jaramillo, W. James, M. Knight, M. W. Carroll, D. Skelly, C. Dold, Y. Peng, R. Levin, T. Dong, A. J. Pollard, J. C. Knight, P. Klennerman, N. Temperton, D. R. Hall, M. A. Williams, N. G. Paterson, F. K. Bertram, C. A. Siebert, D. K. Clare, A. Howe, J. Radecke, Y. Song, A. R. Townsend, K.-Y. A. Huang, E. E. Fry, J. Mongkolsapaya, M. S. Diamond, J. Ren, D. I. Stuart, and G. R. Screaton, The antigenic anatomy of sars-cov-2 receptor binding domain, *Cell* **184**, 2183 (2021).
- [22] J. A. G. de Visser and J. Krug, Empirical fitness landscapes and the predictability of evolution, *Nature Reviews Genetics* **15**, 480 (2014).
- [23] J. F. C. Kingman, A simple model for the balance between selection and mutation, *Journal of Applied Probability* **15**, 1 (1978).
- [24] S. Franz, L. Peliti, and M. Sellitto, An evolutionary version of the random energy model, *Journal of Physics A: Mathematical and General* **26**, L1195 (1993).
- [25] S. A. Kauffman and E. D. Weinberger, The nk model of rugged fitness landscapes and its application to maturation of the immune response, *Journal of Theoretical Biology* **141**, 211 (1989).
- [26] T. Aita, H. Uchiyama, T. Inaoka, M. Nakajima, T. Kokubo, and Y. Husimi, Analysis of a local fitness landscape with a model of the rough mt. fuji-type landscape: Application to prolyl endopeptidase and thermolysin, *Biopolymers* **54**, 64 (2000).
- [27] C. Blanco, E. Janzen, A. Pressman, R. Saha, and I. A. Chen, Molecular fitness landscapes from high-coverage sequence profiling, *Annual Review of Biophysics* **48**, 1 (2019), pMID: 30601678, <https://doi.org/10.1146/annurev-biophys-052118-115333>.
- [28] A. M. Phillips, K. R. Lawrence, A. Moulana, T. Dupic, J. Chang, M. S. Johnson, I. Cvijovic, T. Mora, A. M. Walczak, and M. M. Desai, Binding affinity landscapes constrain the evolution of broadly neutralizing anti-influenza antibodies, *eLife* **10**, e71393 (2021).
- [29] A. M. Phillips, D. P. Maurer, C. Brooks, T. Dupic, A. G. Schmidt, and M. M. Desai, Hierarchical sequence-affinity landscapes shape the evolution of breadth in an anti-influenza receptor binding site antibody, *eLife* **12**, e83628 (2023).
- [30] R. M. Adams, J. B. Kinney, A. M. Walczak, and T. Mora, Epistasis in a fitness landscape defined by antibody-antigen binding free energy, *Cell Systems* **8**, 10.1016/j.cels.2018.12.004 (2019).
- [31] M. C. Julian, L. Li, S. Garde, R. Wilen, and P. M. Tessier, Efficient affinity maturation of antibody variable domains requires co-selection of compensatory mutations to maintain thermodynamic stability, *Scientific Reports* **7**, 10.1038/srep45259 (2017).
- [32] B. Derrida, Random-energy model: Limit of a family of disordered models, *Phys. Rev. Lett.* **45**, 79 (1980).
- [33] B. Derrida, Random-energy model: An exactly solvable model of disordered systems, *Phys. Rev. B* **24**, 2613 (1981).
- [34] We make here the simplifying assumption that d is constant.
- [35] W. König, *The Parabolic Anderson Model: Random Walk in Random Potential*, Pathways in Mathematics (Birkhäuser Cham, 2016).
- [36] L. Avena, O. Gün, and M. Hesse, The parabolic anderson

- model on the hypercube, *Stochastic Processes and their Applications* **130**, 3369 (2020).
- [37] J. M. J. Tas, L. Mesin, G. Pasqual, S. Targ, J. T. Jacobsen, Y. M. Mano, C. S. Chen, J.-C. Weill, C.-A. Reynaud, E. P. Browne, M. Meyer-Hermann, and G. D. Victora, Visualizing antibody affinity maturation in germinal centers, *Science* **351**, 1048 (2016), <https://www.science.org/doi/pdf/10.1126/science.aad3439>.
- [38] J. Lee, D. R. Boutz, V. Chromikova, M. G. Joyce, C. Vollmers, K. Leung, A. P. Horton, B. J. DeKosky, C.-H. Lee, J. J. Lavinder, E. M. Murrin, C. Chrysostomou, K. H. Hoi, Y. Tsybovsky, P. V. Thomas, A. Druz, B. Zhang, Y. Zhang, L. Wang, W.-P. Kong, D. Park, L. I. Popova, C. L. Dekker, M. M. Davis, C. E. Carter, T. M. Ross, A. D. Ellington, P. C. Wilson, E. M. Marcotte, J. R. Mascola, G. C. Ippolito, F. Krammer, S. R. Quake, P. D. Kwong, and G. Georgiou, Molecular-level analysis of the serum antibody repertoire in young adults before and after seasonal influenza vaccination, *Nature Medicine* **22**, 1456 (2016).
- [39] S. N. Majumdar, A. Pal, and G. Schehr, Extreme value statistics of correlated random variables: A pedagogical review, *Physics Reports* **840**, 1 (2020), extreme value statistics of correlated random variables: A pedagogical review.
- [40] H. J. Hilhorst, Central limit theorems for correlated variables: some critical remarks, *Brazilian Journal of Physics* **39**, 371–379 (2009).
- [41] B. V. Gnedenko and A. N. Kolmogorov, *Limit distributions for sums of independent random variables*, Addison-Wesley Mathematics Series (Addison-Wesley, 1954).
- [42] J.-Y. Fortin and M. Clusel, Applications of extreme value statistics in physics, *Journal of Physics A: Mathematical and Theoretical* **48**, 183001 (2015).
- [43] Y.-F. Hu, J.-C. Hu, H.-R. Gong, A. Danchin, R. Sun, H. Chu, I. F.-N. Hung, K. Y. Yuen, K. K.-W. To, B.-Z. Zhang, T. Yau, and J.-D. Huang, Computation of antigenicity predicts sars-cov-2 vaccine breakthrough variants, *Frontiers in Immunology* **13**, 10.3389/fimmu.2022.861050 (2022).
- [44] A. J. Greaney, T. N. Starr, P. Gilchuk, S. J. Zost, E. Binshstein, A. N. Loes, S. K. Hilton, J. Huddleston, R. Eguia, K. H. Crawford, A. S. Dingens, R. S. Nargi, R. E. Sutton, N. Suryadevara, P. W. Rothlauf, Z. Liu, S. P. Whelan, R. H. Carnahan, J. Crowe, James E., and J. D. Bloom, Complete mapping of mutations to the sars-cov-2 spike receptor-binding domain that escape antibody recognition, *Cell Host and Microbe* **29**, 44 (2021).
- [45] We choose to define $\hat{\Delta}_N$ in a non-symmetric way for reasons that will be clear in the study of the parametric 3-class problem, Sec. III 2.
- [46] A. Amir, An elementary renormalization-group approach to the generalized central limit theorem and extreme value distributions, *Journal of Statistical Mechanics: Theory and Experiment* **2020**, 013214 (2020).
- [47] G. Jona-Lasinio, The renormalization group: A probabilistic view, *Il Nuovo Cimento* **26 B**, 99 (1975).
- [48] G. Jona-Lasinio, Renormalization group and probability theory, *Physics Reports* **352**, 439 (2001), renormalization group theory in the new millennium. III.
- [49] D. Li and Y. G. Sinai, An application of the renormalization group method to stable limit laws, *Journal of Statistical Physics* **157**, 10.1007/s10955-014-1098-4 (2014).
- [50] G. Györgyi, N. R. Moloney, K. Ozogány, and Z. Rácz, Finite-size scaling in extreme statistics, *Phys. Rev. Lett.* **100**, 210601 (2008).
- [51] G. Györgyi, N. R. Moloney, K. Ozogány, Z. Rácz, and M. Droz, Renormalization-group theory for finite-size scaling in extreme statistics, *Phys. Rev. E* **81**, 041135 (2010).
- [52] I. Calvo, J. C. Cuchí, J. G. Esteve, and F. Falceto, Extreme-value distributions and renormalization group, *Phys. Rev. E* **86**, 041109 (2012).
- [53] One can reconstruct the phase diagram $P_{fix,C}$ in the plane of control parameters $(\tilde{\Delta}_0, \tilde{\Sigma}_0)$ when $\gamma_V(s) = \gamma_C(s) \rightarrow \gamma > 0$, but it will not exhibit a sharp phase transition. Even in the $N \rightarrow \infty$ limit, $P_{fix,C}$ will be a smooth function of $\tilde{\Sigma}_0$, which must be reconstructed by calculating Eq. (15) along the fixed point line.
- [54] R. A. Fisher and L. H. C. Tippett, Limiting forms of the frequency distribution of the largest or smallest member of a sample, *Mathematical Proceedings of the Cambridge Philosophical Society* **24**, 180–190 (1928).
- [55] M. V. Beek, M. C. Nussenzweig, and A. K. Chakraborty, Two complementary features of humoral immune memory confer protection against the same or variant antigens, *Proceedings of the National Academy of Sciences* **119**, e2205598119 (2022), <https://www.pnas.org/doi/pdf/10.1073/pnas.2205598119>.
- [56] T. Ramaraj, T. Angel, E. A. Dratz, A. J. Jesaitis, and B. Mumey, Antigen–antibody interface properties: Composition, residue interactions, and features of 53 non-redundant structures, *Biochimica et Biophysica Acta (BBA) - Proteins and Proteomics* **1824**, 520 (2012).
- [57] A. Amitai, L. Mesin, G. D. Victora, M. Kardar, and A. K. Chakraborty, A population dynamics model for clonal diversity in a germinal center, *Frontiers in Microbiology* **8**, 10.3389/fmicb.2017.01693 (2017).
- [58] M. O. Altman, J. R. Bennink, J. W. Yewdell, and B. R. Herrin, Lamprey vlrp response to influenza virus supports universal rules of immunogenicity and antigenicity, *eLife* **4**, e07467 (2015).
- [59] E. Engelhart, R. Emerson, L. Shing, C. Lennartz, D. Guion, M. Kelley, C. Lin, R. Lopez, D. Younger, and M. E. Walsh, A dataset comprised of binding interactions for 104,972 antibodies against a sars-cov-2 peptide, *Scientific Data* **9**, 10.1038/s41597-022-01779-4 (2022).
- [60] Q. He, L. Wu, Z. Xu, X. Wang, Y. Xie, Y. Chai, A. Zheng, J. Zhou, S. Qiao, M. Huang, G. Shang, X. Zhao, Y. Feng, J. Qi, G. F. Gao, and Q. Wang, An updated atlas of antibody evasion by sars-cov-2 omicron sub-variants including bq.1.1 and xbb, *Cell Reports Medicine* **4**, 100991 (2023).
- [61] S. M. Moin, J. C. Boyington, S. Boyoglu-Barnum, R. A. Gillespie, G. Cerutti, C. S.-F. Cheung, A. Cagigi, J. R. Gallagher, J. Brand, M. Prabhakaran, Y. Tsybovsky, T. Stephens, B. E. Fisher, A. Creanga, S. Ataca, R. Rawi, K. S. Corbett, M. C. Crank, J. Gorman, A. B. McDermott, A. K. Harris, T. Zhou, P. D. Kwong, L. Shapiro, J. R. Mascola, B. S. Graham, and M. Kanekiyo, Vaccine-elicitation of cross-group neutralizing protective antibodies to influenza A viruses, *bioRxiv* 10.1101/2022.02.11.480115 (2022), <https://www.biorxiv.org/content/early/2022/02/12/2022.02.11.480115>.
- [62] J. K. Hwang, F. W. Alt, and L.-S. Yeap, Related mechanisms of antibody somatic hypermutation and class

- switch recombination, *Microbiology Spectrum* **3**, 10.1128 (2015).
- [63] J. M. Di Noia and M. S. Neuberger, Molecular mechanisms of antibody somatic hypermutation, *Annual Review of Biochemistry* **76**, 1 (2007), PMID: 17328676.
- [64] N. Spisak, A. M. Walczak, and T. Mora, Learning the heterogeneous hypermutation landscape of immunoglobulins from high-throughput repertoire data, *Nucleic Acids Research* **48**, 10702 (2020).